Numerical analysis of electrically tunable aspherical optofluidic lenses

Kartikeya Mishra and Frieder Mugele

Physics of Complex Fluids, Department of Science and Technology, IMPACT and MESA + Institute, University of Twente, P. O. Box 217, 7500 AE, Enschede, The Netherlands
*f.mugele@utwente.nl

Abstract: In this work, we use the numerical simulation platform Zemax to investigate the optical properties of electrically tunable aspherical liquid lenses, as we recently reported in an experimental study [K. Mishra, C. Murade, B. Carreel, I. Roghair, J. M. Oh, G. Manukyan, D. van den Ende, and F. Mugele, "Optofluidic lens with tunable focal length and asphericity," Sci. Rep. **4**, 6378 (2014)]. Based on the measured lens profiles in the presence of an inhomogeneous electric field and the geometry of the optical device, we calculate the optical aberrations, focusing in particular on the Z11 Zernike coefficient of spherical aberration obtained at zero defocus (Z4). Focal length and spherical aberrations are calculated for a wide range of control parameters (fluid pressure and electric field), parallel with the experimental results. Similarly, the modulation transfer function (MTF), image spot diagrams, Strehl's ratio, and peak-to-valley (P–V) and root mean square (RMS) wavefront errors are calculated to quantify the performance of our aspherical liquid lenses. We demonstrate that the device concept allows compensation for a wide range of spherical aberrations encountered in optical systems.

OCIS codes: (230.0230) Optical devices; (230.2090) Electro-optical devices; (000.4430) Numerical approximation and analysis; (220.1080) Active or adaptive optics; (220.1000) Aberration compensation.

References and links

1. H. W. Yoo, M. Verhaegen, M. E. van Royen, and G. Schitter, "Automated Adjustment of Aberration Correction in Scanning Confocal Microscopy," in *Proceeding of IEEE on International Instrumentation and Measurement Technology Conference* (IEEE, 2012), pp.1083–1088 (2012).
2. K. Mishra, C. Murade, B. Carreel, I. Roghair, J. M. Oh, G. Manukyan, D. van den Ende, and F. Mugele, "Optofluidic lens with tunable focal length and asphericity," Sci. Rep. **4**, 6378 (2014).
3. N. T. Nguyen, "Micro-optofluidic lenses: a review," Biomicrofluidics **4**(3), 031501 (2010).
4. A. Werber and H. Zappe, "Tunable microfluidic microlenses," Appl. Opt. **44**(16), 3238–3245 (2005).
5. C. P. Chiu, T. J. Chiang, J. K. Chen, F. C. Chang, F. H. Ko, C. W. Chu, S. W. Kuo, and S. K. Fan, "Liquid lenses and driving mechanisms: a review," J. Adhes. Sci. Technol. **26**(12–17), 1773–1788 (2012).
6. M. Pan, M. Kim, S. Kuiper, and S. K. Y. Tang, "Actuating fluid-fluid interfaces for the reconfiguration of light," IEEE J. Sel. Top. Quantum Electron. **21**(4), 9100612 (2015).
7. C.-C. Cheng and J. Andrew Yeh, "Dielectrically actuated liquid lens," Opt. Express **15**(12), 7140–7145 (2007).
8. H. Yu, G. Zhou, H. M. Leung, and F. S. Chau, "Tunable liquid-filled lens integrated with aspherical surface for spherical aberration compensation," Opt. Express **18**(10), 9945–9954 (2010).
9. S. H. Cho, F. S. Tsai, W. Qiao, N. H. Kim, and Y. H. Lo, "Fabrication of aspherical polymer lenses using a tunable liquid-filled mold," Opt. Lett. **34**(5), 605–607 (2009).
10. P. P. Zhao, C. Ataman, and H. Zappe, "An endoscopic microscope with liquid-tunable aspheric lenses for continuous zoom capability," Proc. SPIE **9130**, 913004 (2014).
11. Z. Zhan, K. Wang, H. Yao, and Z. Cao, "Fabrication and characterization of aspherical lens manipulated by electrostatic field," Appl. Opt. **48**(22), 4375–4380 (2009).
12. S. M. Kuo and C. H. Lin, "Fabrication of aspherical SU-8 microlens array utilizing novel stamping process and electro-static pulling method," Opt. Express **18**(18), 19114–19119 (2010).
13. G. I. Kweon and C. H. Kim, "Aspherical lens design by using a numerical analysis," J. Korean Phys. Soc. **51**(1), 93–103 (2007).

#263021 Received 13 Apr 2016; revised 13 May 2016; accepted 15 May 2016; published 21 Jun 2016

14. Z. L. Cao, C. Cheng, and K. Y. Wang, "Numerical simulation on aspherical lens modulated by electrostatic force," Proc. SPIE **9281**, 92810H (2014).
15. S. Reichelt and H. Zappe, "Design of spherically corrected, achromatic variable-focus liquid lenses," Opt. Express **15**(21), 14146–14154 (2007).
16. H. Zhao, "Optical ensemble analysis of intraocular lens performance through a simulated clinical trial with ZEMAX," Opt. Lett. **34**(1), 7–9 (2009).
17. Y. K. Fuh and P. W. Chen, "Novel dual-function lens with microscopic and vari-focus capability incorporated with an aberration-suppression aspheric lens," Opt. Express **23**(17), 21771–21785 (2015).
18. N. C. Lima, A. Cavalli, K. Mishra, and F. Mugele, "Numerical simulation of astigmatic liquid lenses tuned by a stripe electrode," Opt. Express **24**(4), 4210–4220 (2016).
19. Y. H. Gao, Z. Q. Yang, W. X. Zhao, B. Jiang, D. M. Li, and M. S. Li, "Optimum design of cam curve of zoom system based on Zemax," Optik (Stuttg.) **124**(23), 6358–6362 (2013).
20. R. A. Flynn, E. F. Fleet, G. Beadie, and J. S. Shirk, "Achromatic GRIN singlet lens design," Opt. Express **21**(4), 4970–4978 (2013).
21. J. M. Oh, G. Manukyan, D. van den Ende, and F. Mugele, "Electric-field-driven instabilities on superhydrophobic surfaces," Europhys. Lett. **93**(5), 56001 (2011).
22. I. Roghair, M. Musterd, D. van den Ende, C. R. Kleijn, M. Kreutzer, and F. Mugele, "A numerical technique to simulate display pixels based on electrowetting," Microfluid. Nanofluidics **19**(2), 465–482 (2015).
23. Q. H. Li and X. P. Shao, "Spherical aberration and modulation transfer function," Proc. SPIE **9124**, 91241B (2014).
24. P. Zhao, Ç. Ataman, and H. Zappe, "Spherical aberration free liquid-filled tunable lens with variable thickness membrane," Opt. Express **23**(16), 21264–21278 (2015).

1. Introduction

Optical aberrations are usually encountered in areas like imaging, photography, and microscopy. Their presence degrades the optical quality of the captured image, rendering it unfit for use in many professional applications. In order to mitigate optical aberrations, it is often necessary to build more complex optical systems composed of multiple optical elements. Of all the optical aberrations commonly observed, spherical aberration is the most fundamental. In microscopy, for example, specimen is routinely imaged through coverslips, which induces considerable spherical aberration. In order to compensate for this, one has to resort to either immersion objectives, such that the refractive index of the imaging medium is equal to that of the glass coverslip, or to dry objectives, in which a correction collar is employed to minimize the aberration. This is particularly true for high NA objectives, which require correction collars that have to be adjusted all the time [1]. This makes the optical systems bulky, difficult to build, and also expensive. Moreover, industrially manufactured solid lenses have a fixed focal length and are non-tunable in nature.

Various numerical schemes have been proposed to evaluate spherical aberration. Optical simulation platforms, such as Zemax, are routinely employed to design aspherical lenses [13, 14] and spherically corrected achromatic variable-focus liquid lenses [15] for superior optical performance. Such tools offer the opportunity to estimate the optical properties of lenses in order to gauge their optical performance prior to construction. They also give us flexibility to optimize the design parameters according to specific customized requirements. Intra-ocular lenses [16] have also been designed and developed using Zemax to provide solutions in ophthalmic applications. Fuh and Chen [17] designed and constructed an optical system comprising an aspheric PDMS lens with aberration control properties. Lima et al. [18] numerically estimated the optical properties of electrically tunable astigmatic lenses. This was achieved employing a stripe electrode, thereby introducing rotational asymmetry in the lens meniscus, which was eventually manifested in the astigmatic behavior of the lens. Such lenses are of potential use in correcting ocular astigmatism. Continuous zoom lenses [19] with real time MTF evaluation and achromatic GRIN singlet lenses [20] have also been conceptualized in Zemax.

In this work, we employ Zemax to analyze the optical performance of our electrically tunable aspherical lenses, as reported by Mishra et al. [2]. There, we presented a design and demonstrated experimentally that spherical aberration can be suppressed by the application of a voltage. However, the characterization of the optical properties of liquid lenses was rather

#263021 Received 13 Apr 2016; revised 13 May 2016; accepted 15 May 2016; published 21 Jun 2016

crude: we simply calculated the longitudinal spherical aberration (LSA) by comparing the focal length of the paraxial beams and marginal beams based on side-view images of the liquid-liquid interface and the refractive indices of the two phases. This is a rather incomplete estimate, which ignores various other parts of the device, such as the unavoidable top and bottom plates covering the liquid lens. Here, we present a complete picture of the lens characterization, by investigating wavefront aberrations—specifically, Zernike spherical aberration (Z11)—and other pertinent optical properties, such as modulation transfer function (MTF) and image spot size. Z11 is calculated in units of waves, signifying the phase difference.

2. Methods

We analyzed the optical properties of our device based on the captured side-view images of the liquid lens, by extracting their respective surface profiles, fitting them with a conic section, and extracting their geometrical properties: eccentricity and radius of curvature at apex. Figure 1(a) depicts the schematic of the experimental setup employed by Mishra et al. [2]. The device consists of a top glass plate (light blue in Fig. 1(a)) with a thin transparent ITO electrode (not shown in Fig. 1(a)), gold-coated aperture plate (dark yellow in Fig. 1(a)) and bottom glass plate (white in Fig. 1(a)). Conductive aqueous lens fluid (blue in Fig. 1(a)) is entrapped in an O-ring (black in Fig. 1(a)), sandwiched between the aperture plate and bottom glass plate, and an electrically insulating phase (yellow in Fig. 1(a)) of silicon oil is contained between the aperture plate and top glass plate. Lens meniscus is created via hydrostatic pressure in an ambient silicon oil environment. The aperture diameter is 1 mm, and the distance between the aperture plate and top electrode is 2 mm. The meniscus is pinned along the aperture by a hydrophobic-hydrophilic contact.

The lens shape is controlled by two driving mechanisms: hydrostatic pressure and electric field. The meniscus profile at zero voltage is manipulated by simply tuning the hydrostatic pressure. The asphericity in the lens meniscus is induced by applying the voltage between the aperture plate and top electrode. The aqueous phase is kept at a fixed potential throughout the experiment. The ratio of refractive index of lens fluid to ambient silicon oil is 1.10. Further details of the lens device can be found elsewhere [2]. Figure 1(b) shows a side-view of one such aspherical lens under an applied voltage.

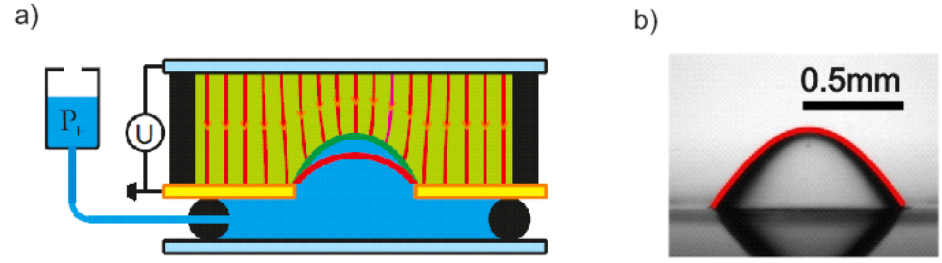

Fig. 1. a) Schematic of electrically tunable optofluidic lens setup. A spherical lens created via hydrostatic pressure (ΔPh) is deformed into an aspherical shape by an application of a voltage (U) between the aperture plate and top electrode. Red curves spanning between the aperture plate and top electrode signify electric field lines. b) Side-view of aspherical lens under an applied voltage. The red curve shows the conic section fit.

Oh et al. [21] investigated the evolution of liquid interface into aspherical configurations of varying eccentricities under the influence of an electric field. The equilibrium lens profiles is determined by the balance of the applied hydrostatic pressure P_h, the Laplace pressure $\Delta P_L = 2\gamma\kappa(r)$ (γ: surface tension; $\kappa(r)$: local curvature of the interface) and the local Maxwell stress $\Pi_{el}(r) = \epsilon\epsilon_0 E^2/2$ according to:

#263021 Received 13 Apr 2016; revised 13 May 2016; accepted 15 May 2016; published 21 Jun 2016

$$P_h = 2\gamma\kappa(r) - \Pi_{el}(r)$$

($\varepsilon\varepsilon_0$ is the dielectric permittivity of the oil. $E(r)$ is the electric field at the location r.). Roghair et al. [22] formulated a numerical scheme to compute such equilibrium interfaces between conductive and non-conductive fluids.

Figure 2 illustrates the optical simulation setup, in which each element of the lens device (shown in Fig. 1(a) is represented by a corresponding section of the similar material with its geometric thickness and shape as well as refractive index (note that the dimensions in Fig. 2 are not to scale). The objective is to characterize the optical performance of the lens device for variable hydrostatic pressure ΔP_h and voltage U by calculating the Zernike spherical aberration (Z11) under zero defocus (Z4) conditions. The experimental values of lens meniscus curvature, aperture size, and eccentricity, along with other device parameters—such as the thickness and refractive index of the glass and the distances between the subsequent optical elements—are defined as constant input parameters in the lens data editor (LDE) of the Zemax simulation toolbox. Green light at λ = 534nm is employed in the simulation to illuminate the lens aperture. The following table summarizes the materials, thicknesses, and refractive indices of the various lens device mediums.

Table 1. Specifications of lens device sections: material, thickness and refractive index

Section Number	Material	Thickness (mm)	Refractive index
1	Glass	1	1.51
2	Silicon oil	2	1.40
3	Conductive aq. solution	1	1.55
4	Glass	1	1.51

The distance between the top glass plate (1) and point object (f_0) is defined as the variable and is optimized for zero defocus. The distance between the bottom glass plate (4) and image plane (5) is kept stationary for all the simulations. Z11 is evaluated with respect to a reference planar wavefront. Any particular optical system is optimized for its particular optical merit as defined by merit function. In our case, defocus aberration (Z4) is the merit function. The optimization routine is executed to estimate the optimized numerical value of f_0, for Z4 equal to zero. The optimized value of the variable f_0 is calculated for the different values of hydrostatic pressure ΔP_h and voltage U.

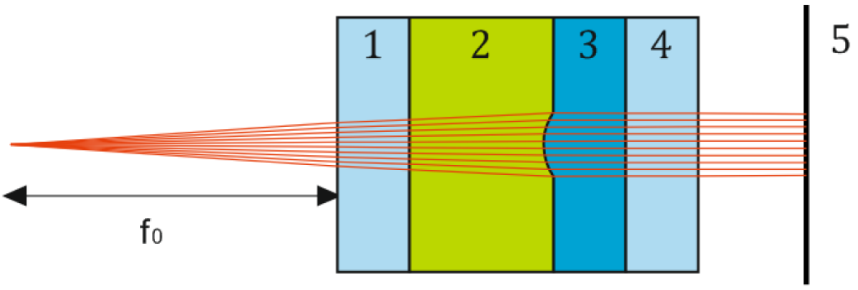

Fig. 2. Simulation set-up of an optofluidic lens device in Zemax. A liquid lens is produced by hydrostatic pressure through an aperture of 1-mm diameter. Sections of the device are numbered as follows: 1-Top glass plate with 30-nm coated ITO, 2-Silicon oil, 3-Electrically conductive aqueous solution, 4-Bottom glass plate, and 5-Image plane. The material, thickness, and refractive indices of the device sections are summarized in Table 1.

In simulations, the f_0 lies in air. Compared to our previous estimate [2], in which we calculated the longitudinal spherical aberration (LSA) solely on the basis of the shape of the lens surface, this analysis also includes the optical effect of the top and bottom glass plates,

#263021 Received 13 Apr 2016; revised 13 May 2016; accepted 15 May 2016; published 21 Jun 2016

which are integral elements of the actual lens device. Moreover, by calculating Z11, we quantify the actual wavefront aberrations, whereas the LSA merely signifies geometrical aberrations.

3. Results and discussions

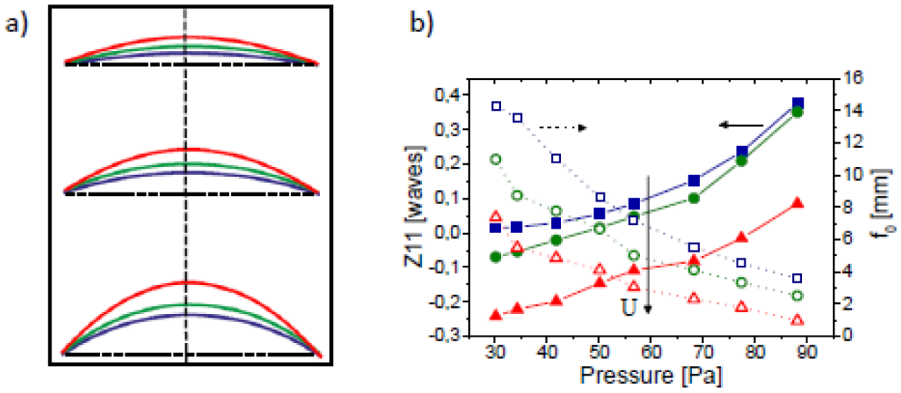

Fig. 3. a) Lens profiles at ΔP_h = 30 Pa (blue), 56 Pa (green), and 88 Pa (red) for different values of U: 0 V (top), 1.73 kV (middle), and 2.45 kV (bottom). b) Variation of f_0 (open symbols) and Zernike spherical aberration (closed symbols) versus ΔP_h for U = 0V (squares), 1.73 kV (circles), and 2.45 kV (triangles).

Figure 3(a) illustrates the lens profiles as extracted from the side-view images captured under different combinations of ΔP_h and U. Figure 3(b) depicts the variations of Z11 and f_0 against the applied hydrostatic pressure. At zero voltage, the drop assumes a spherical cap shape with a radius R, as required by the balance of the Laplace pressure ΔP_L and the hydrostatic pressure, *i.e.* $\Delta P_L = 2\gamma / R = P_h$. As thehydrostatic pressure P_h is increased, the curvature of the lens meniscus increases, retaining its spherical character. Consequently, f_0 decreases, which in turn enhances spherical aberration. This is evident from Fig. 3. As hydrostatic pressure is increased from 30 Pa to 88 Pa at zero voltage (U = 0V), f_0 changes from 14.3 mm to 3.59 mm. Simultaneously, Z11 increases from 0.015 waves at 30 Pa to 0.38waves at 88 Pa. As U is raised, the shape of the lens changes from spherical at 0V to aspherical configurations at higher voltages. This is clearly evident in Fig. 3(a), where, starting from the spherical meniscus at 0 V, the lens assumes aspherical profiles at higher voltages.

These trends are consistent with the results reported by Mishra et al. [2], where the LSA was shown to increase with the hydrostatic pressure for a spherical lens shape at zero voltage. Similar trends in focal lengths and Zernike spherical aberration (Z11) are observed as a finite voltage is applied between the aperture plate and top electrode. For $U \neq 0$V, the meniscus assumes aspherical shapes with changing eccentricities. For U = 1.73kV, f_0 (open circles) varies from 10.96 mm to 2.52 mm, while Z11 (closed circles) changes from –0.069 waves to 0.35waves. Similarly, for U = 2.45kV, f_0 (open triangles) varies from 7.38 mm to 0.97 mm, and Z11 (closed triangles) varies from -0.24 waves to 0.085 waves. Clearly, as is evident from Fig. 3(b), for $U \neq 0$V, the Z11 coefficient initially assumes negative values. As we increase the ΔP_h, Z11 eventually attains positive values.

Figure 4 shows the variation of f_0 against the square of U for various initial values of hydrostatic pressures. Upon applying a voltage between the top electrode and aperture plate, the optimized value of f_0 decreases as the point source moves towards the top electrode. In the process, the lens assumes a hyperbolic shape, with its eccentricity matching the ratio of the refractive index of the lens fluid and ambient silicon oil, thus producing a perfect lens with minimum spherical aberration. The entire plot can be divided into two broadly distinct zones,

#263021 Received 13 Apr 2016; revised 13 May 2016; accepted 15 May 2016; published 21 Jun 2016

one with positive values of the Zernike spherical aberration coefficient (Z11) and the other with negative values. The former corresponds to surface profiles with eccentricities less than a perfect aspherical lens, the latter to higher eccentricities. The green line connects the meniscus profiles with zero values of Z11. Hence, such lenses exhibit superior optical quality. The two red lines connect the negative values of the Z11 = –0.1waves and of the Z11 = –0.2waves. Similarly, the magenta lines connect the positive values of the Z11 = 0.1waves and of the Z11 = 0.2waves.

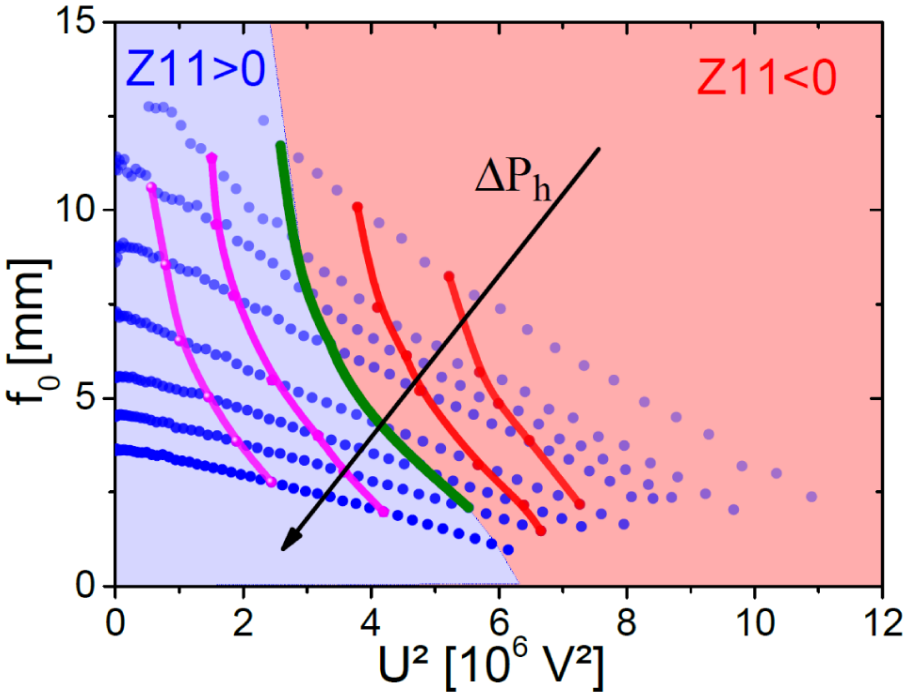

Fig. 4. Variation of f_0 with voltage squared (blue circles) for ranges of ΔPh = 30 Pa, 34 Pa, 42 Pa, 50 Pa, 56 Pa, 68 Pa, 77 Pa, and 88 Pa. Increasing the color gradient of blue circles delineates increase in hydrostatic pressure. The green curve depicts lens profiles with zero values of Z11. Red lines connect the profiles of the Z11 = –0.1waves and the Z11 = 0.2waves, while magenta lines show the profiles of the Z11 = 0.1waves and the Z11 = 0.2waves.

It is important to note the effect of the top and bottom glass plates on the numerical values of f_0 and Z11. Changing the thickness of the top and bottom plates or simulating the device under the semi-infinite oil and water phase results in a focal shift; that is, it changes the value of f_0. However, the values of Z11 remain approximately the same. For example, by changing the thickness of the top plate from 1 mm to 2 mm at 68 Pa under the applied voltage of 2.24 kV, Z11 changes insignificantly from 0.08586 waves to 0.085233 waves, and f_0 changes from 2.96 mm to 2.28 mm. However, the numerical value of the Z11 coefficient remains unaltered by varying the thickness of the bottom plate.

In order to further assess the optical quality of our liquid lenses, we generated the modulation transfer function (MTF) curves to quantify their resolution. Figure 5(a) shows the MTF plot for spherical lenses at four different values of ΔP_h. MTF is plotted against the angular frequency for different values of initial hydrostatic pressures. The black curve signifies the diffraction-limited system corresponding to the best resolved system under given design constraints. The higher the departure of the MTF curve from the diffraction-limited black curve, the larger the spherical aberration and hence more degenerated the optical quality [23]. It is evident from the plot that MTF degrades with increasing backpressure. This is in

#263021 Received 13 Apr 2016; revised 13 May 2016; accepted 15 May 2016; published 21 Jun 2016

agreement with the fact that an increase in backpressure aggravates the spherical aberration of the lens meniscus, thus producing optically inferior lenses with substantially reduced MTF.

However, as a voltage is applied between aperture plate and top electrode, the spherical aberration reduces and is perfectly compensated at a specific hyperbolic shape, producing an MTF curve approaching the diffraction-limited curve at a particular pressure-dependent optimum voltage $U(\Delta P_h)$. This occurs at a voltage when the eccentricity of the lens profile matches with the refractive index ratio of the lens fluid to that of ambient silicon oil medium. As the voltage is increased further, the lens shape again departs from the perfect lens, thereby producing aspherical lenses of inferior optical quality. Figure 5(b) represents the MTF plot of an aspherical lens corresponding to an initial backpressure of 68 Pa at varying values of voltage. Figure 5(c) depicts the MTF curves of perfect lenses for different values of initial hydrostatic pressures. As is evident from the plot, the curves approximately fall on the diffraction-limited MTF indicating ideal lens behavior, signifying superior optical quality.

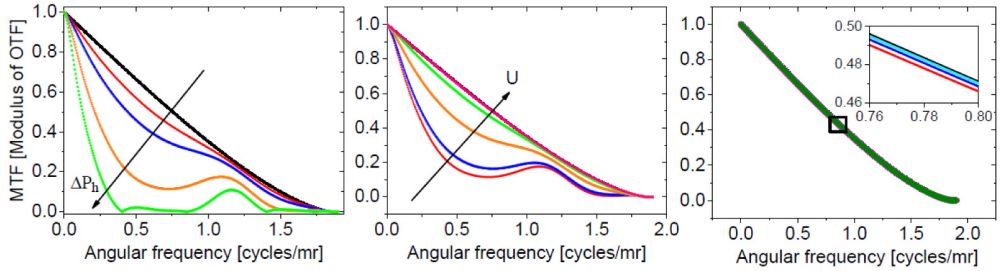

Fig. 5. a) MTF versus angular frequency for four different values of hydrostatic pressure under zero voltage: 50 Pa (red), 56 Pa (blue), 68 Pa (orange), and 77 Pa (green). The black curve depicts diffraction-limited MTF. b) MTF versus angular frequency as voltage is applied at 0 kV (red), 1.32 kV (blue), 1.95 kV (orange), 2.12 kV (green), and 2.18 kV (pink) for ΔPh = 68Pa. c) MTF curves of perfect lenses corresponding to four different values of ΔPh: 50 Pa (red), 56 Pa (blue), 68 Pa (orange), and 77 Pa (green). The inset shows the enlarged view of a section (black box) of superimposed MTF curves.

Other metrics with which to judge the optical quality employ spot diagram, Strehl's ratio, and peak-to-valley (P–V) and RMS wavefront values. Spot diagram depicts the distribution of rays on the image plane. If the spot diagram lies entirely within the airy disc (black circles in Fig. 6), the system is said to be diffraction-limited. In our case, the airy disc diameter is 6.52 mrad. Figure 6(a) illustrates the variation in RMS spot diameter and geometrical (GEO) spot diameter as hydrostatic pressure is increased from 50 Pa to 76 Pa. The corresponding values of spot diameters are tabulated in Table 2 (top). As is evident, the RMS and GEO spot diameters increase by increasing the pressure, eventually spanning outside the airy disc and thereby signifying degradation in image quality. The degeneration in optical quality is consistent with the degradation in resolution as discussed above regarding the MTF plot (see Fig. 5(a)). Figure 6(b) shows the spot diagram for the same conditions as the MTF plot in Fig. 5(b). As expected, the diameter of the spot image decreases upon increasing the applied voltage at a fixed pressure and is finally contained within the airy disc at optimum voltage. Figure 6(c) shows the spot diagrams of perfect lenses for different values of hydrostatic pressures. It is evident that, in all cases, the image spot diagram falls entirely within the airy disc, further corroborating the conclusion made in Fig. 5(c) and highlighting the improved optical performance.

#263021 Received 13 Apr 2016; revised 13 May 2016; accepted 15 May 2016; published 21 Jun 2016

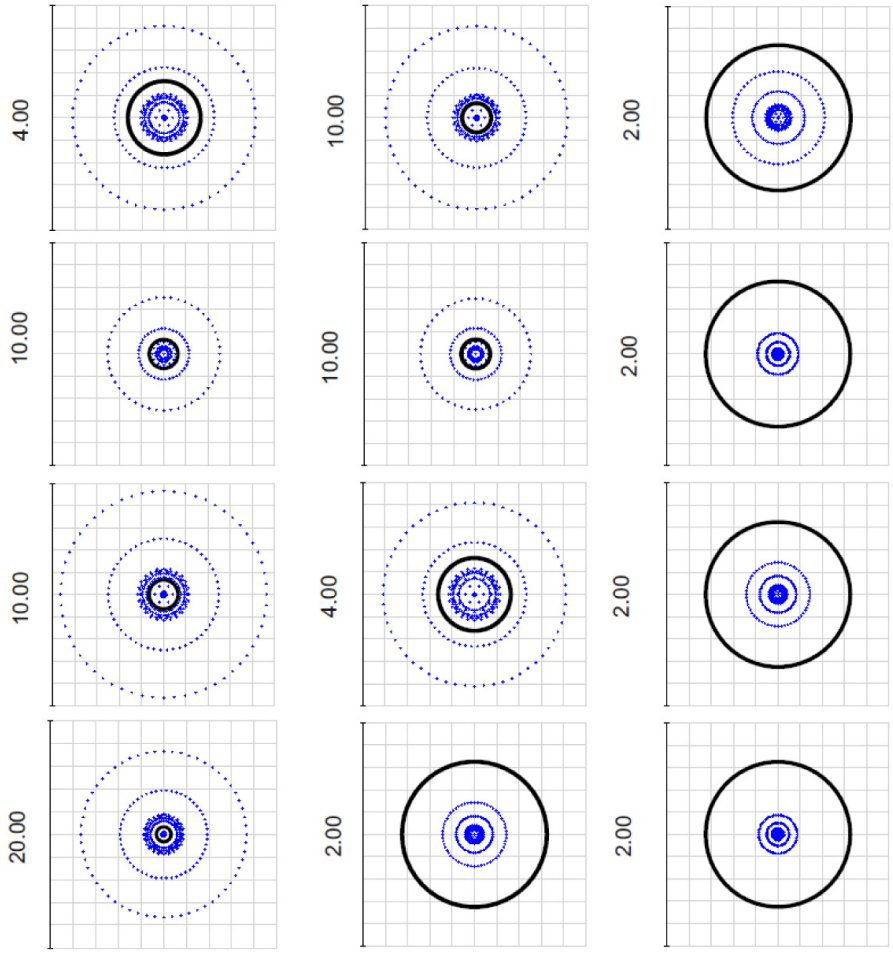

Fig. 6. a) Spot diagrams of spherical lenses under zero voltage at hydrostatic pressures of 50 Pa, 56 Pa, 68 Pa, and 77 Pa. The black circle represents airy disc. b) Spot diagrams of aspherical lenses corresponding to ΔP_h = 68Pa as the voltage is increased from 1.32 kV, 1.95 kV, and 2.12 kV to 2.18 kV. c) Spot diagrams of perfect aspherical lenses with Z11 ≈0, corresponding to different values of ΔP_h: 50 Pa, 56 Pa, 68 Pa, and 77 Pa.

The specific values of the GEO and RMS diameters of the spot images are summarized in Table 2 for a series of conditions. In Table 2, we also provide a series of other merit figures that are commonly used to quantify the quality of optical systems. Specifically, Strehl's ratio gives the ratio of peak intensity of an aberrated system under consideration to the peak intensity of the diffraction-limited system as observed on the image plane from a point source. This varies between 0 and a perfect value of 1. Optical systems with Strehl's ratios of ≥ 0.8 are generally considered as excellent diffraction limited systems. Like the MTF and the spot diagrams, the Strehl's ratio results also indicated that excellent optical performance can be achieved by applying the optimized voltage. Furthermore, we specify the P–V and RMS values of the wavefront aberration as calculated from the wavefront maps. As expected, the errors were reduced to somewhat smaller values at optimum voltages.

#263021 Received 13 Apr 2016; revised 13 May 2016; accepted 15 May 2016; published 21 Jun 2016

Table 2. Optical properties of a) Spherical lenses under zero voltage at hydrostatic pressures of 50 Pa, 56 Pa, 68 Pa and 77 Pa; b) Aspherical lenses corresponding to ΔP_h = 68Pa as voltage is applied from 1.32 kV, 1.95 kV, and 2.12 kV to 2.18 kV; and c) Perfect aspherical lenses under applied voltage corresponding to four different values of hydrostatic pressure: 50 Pa, 56 Pa, 68 Pa, and 77 Pa.

Pressure (Pa)	RMS radius (mrad)	GEO radius (mrad)	SR	P–V (waves)	RMS (waves)
50	0.83	1.64	0.89	0.19	0.056
56	1.34	2.53	0.75	0.29	0.085
68	2.33	4.66	0.39	0.53	0.15
77	3.64	7.31	0.11	0.83	0.24

Voltage (kV)	RMS radius (mrad)	GEO radius (mrad)	SR	P–V (waves)	RMS (waves)
0	2.33	4.66	0.39	0.53	0.15
1.32	2.06	4.09	0.47	0.47	0.14
1.95	1.26	2.48	0.74	0.29	0.087
2.12	0.84	1.64	0.88	0.19	0.059

Pressure (Pa)	RMS radius (mrad)	GEO radius (mrad)	SR	P–V (waves)	RMS (waves)
50	0.21	0.42	0.99	0.05	0.015
56	0.09	0.18	0.99	0.02	0.007
68	0.15	0.29	0.99	0.04	0.01
77	0.09	0.17	0.99	0.02	0.007

4. Conclusion

In this research, we have assessed the optical characteristics of the aspherical lens device reported earlier by Mishra et al. [2]. We formulated a numerical procedure to compute the performance parameters on Zemax, and we concluded that spherical aberration can be subsided and eliminated by the application of a voltage. This is realized by subjecting the liquid meniscus to an electric field. In another study, reported recently by Zhao et al. [24], it was experimentally demonstrated that for tunable elastomeric lenses of 3-mm clear aperture, considerable improvement in optical performance can be achieved over a focal length range of 6 mm to 12 mm. This was further confirmed by evaluating the MTF curves and RMS error. The Strehl's ratio attained was 0.94, signifying diffraction-limited performance. In our case, the range of accessible focal lengths was between 1 mm and 14 mm. Also, as confirmed by various optical metrics, we were able to successfully achieve perfect lens configuration for different initial hydrostatic pressures by application of the voltage.

It is important to highlight the potential use of liquid aspherical lenses. Due to their tunable focal length and ability to reduce optical aberrations, liquid aspherical lenses offer potential applications in imaging. For example, while imaging a point object on a 170-micron coverslip through our lens device at 68 Pa under an applied voltage of 2.25 kV, by optimizing the distance between the coverslip and top glass plate, one can reduce the spherical aberration to less than 0.01waves. Thus, the aberrations introduced in optical microscopy while imaging biological specimens can be compensated by electrical aberration control.

Standard objectives have a fixed numerical aperture and working distance. Aspherical lenses, on the other hand, come with the advantage of tunability. Variable numerical apertures and focal lengths can be achieved by effectively manipulating the hydrostatic pressure and voltage. By choosing fluids of different refractive indices and by optimizing the device design, one can further alter the tuning range of numerical apertures and focal lengths. Moreover, spherical aberration increases with numerical aperture. By applying an electric field and consequently inducing sufficient asphericity, however, it is possible to eliminate the pronounced spherical aberration encountered at higher numerical apertures.

#263021 Received 13 Apr 2016; revised 13 May 2016; accepted 15 May 2016; published 21 Jun 2016

Another advantage of electrically actuated liquid lenses is their operation speed. One can apply a voltage and correct the aberrations in few milliseconds. To improve the optical resolution, it would be desirable to increase the (geometric) aperture of the lens. This has the disadvantage that gravitational distortions of the lens shape, which scale quadratically with the aperture diameter become more important. It is possible, though, to compensate gravitational distortions by the electric field, too. The operation speed is expected to decrease as well, due to the possible excitation of oscillations of the lens surface. Experiments to evaluate the dynamic response and its consequences for the operation of larger lenses are ongoing.

Acknowledgments

We gratefully acknowledge the Dutch Science Foundation NWO and the Foundation for Technical science STW for financial support within the VICI program grant #11380. We would like to extend our thanks to Arjen Pit and Nicolao Lima for helping with the editing of figures.

#263021 Received 13 Apr 2016; revised 13 May 2016; accepted 15 May 2016; published 21 Jun 2016